Available online at www.sciencedirect.com
SCIENCE DIRECT®
ELSEVIER
Journal of Magnetism and Magnetic Materials 305 (2006) 100–109
Journal of magnetism and magnetic materials
www.elsevier.com/locate/jmmm

Synthesis, assembly and physical properties of magnetic nanoparticles ☆

Xiao-Min Lin[a,*], Anna C.S. Samia[b]

[a]Argonne National Laboratory, Materials Science Division, Chemistry Division and Center for Nanoscale Materials, Argonne, IL 60439, USA
[b]Argonne National Laboratory, Chemistry Division, Argonne, IL 60439, USA

Received 26 September 2005; received in revised form 18 November 2005
Available online 9 January 2006

Abstract

Compared with the top-down lithographic techniques, bottom-up chemical synthesis and self-assembly approaches offer much more flexibilities in creating magnetic nanostructures with controlled size, shape, composition and physical properties. This review summarizes some of the latest developments in this field, with emphasis mainly on transition metals, their alloys and metal oxide nanoparticles. The focus is directed towards the conditions of individual particles as well as large assemblies of particles through colloidal chemistry. Furthermore, some of the future directions in nanomagnetism from the perspective of physical chemists is also presented.

PACS: 78.67.Bf; 61.46.+w; 81.16.Dn

Keywords: Magnetic nanoparticles; Colloids; Chemical synthesis; Self-assembly

1. Introduction

Magnetism has fascinated humans for thousands of years, but it is only recently that we began to realize that magnetism is, to a large extent, a nanoscale phenomenon [1]. The atomic exchange interaction that defines ferromagnetism is typically on the length scale of 10 nm for most materials [2]. The competition between the exchange interaction and magnetic anisotropy leads to domain formation, with a domain wall width also in the nanometer region. When the dimensions of the materials become comparable to these length scales, new properties begin to emerge, such as enhanced magnetic moments [3,4], exchanged-coupled dynamics [5], quantization of spin waves [6,7] and giant magnetoresistance [8,9]. These new properties lead to potential applications in permanent magnets, multi-terabit/in^2 data storage devices [10,11], new magnetic refrigeration systems [12], enhancing agents for magnetic resonance imaging [13], catalysis [14] and targeted drug delivery [15]. Research and applications of these unique features of magnetic nanostructures start with the material synthesis and fabrication. During the past two decades, chemical synthesis has demonstrated to be a powerful and rapid venue to obtain large quantities of nanosize building blocks in a single reaction. The magnetic nanostructures obtained through colloidal chemistry have better crystallinity, and are typically much smaller in size than what are typically achieved using top-down lithographic techniques. Particle size can be tuned through varying synthetic conditions. This has provided tremendous opportunities to investigate the transition of magnetism from the atomic scale to the bulk level.

This review focuses on the recent developments of chemically synthesized magnetic nanostructures, with the emphasis mainly on transition metals, alloys and oxides. Even within this limited scope, it is still difficult to cover the entire research field. Furthermore, review articles of this type inevitably reflect the authors' own research interests, and in this case, it is mainly from the perspective

☆The submitted manuscript has been created by the University of Chicago as Operator of Argonne National Laboratory ("Argonne") under Contract No. W-31-109-ENG-38 with the US Department of Energy. The US Government retains for itself, and others acting on its behalf, a paid-up, nonexclusive, irrevocable worldwide license in said article to reproduce, prepare derivative works, distribute copies to the public, and perform publicly and display publicly, by or on behalf of the Government.

*Corresponding author. Tel.: +1 6302526289; fax: +1 6302529151.
E-mail address: xmlin@anl.gov (X.-M. Lin).

0304-8853/$ - see front matter © 2006 Elsevier B.V. All rights reserved.
doi:10.1016/j.jmmm.2005.11.042

of physical chemists. Thus, readers are strongly recommended to refer to several excellent review articles and books that already exist [2,16–20]. Section 2 is devoted to the synthesis of magnetic nanostructures. Section 3 focuses on self-assembly strategies used to create macroscopic materials. Section 4 discusses the magnetic properties that are currently being investigated. And finally, we summarize some of the future research directions in this field.

2. Synthesis

The basic principle of chemical synthesis of nanostructured materials is to initiate chemical reactions and control the nucleation and growth of the reaction products. This can be achieved by conducting the reactions within a confined environment or controlling the reaction process through a dynamic binding of surface ligands. Among various chemical syntheses, two approaches are most successful in creating stable colloids with good size dispersion. Microemulsion-based syntheses are typically carried out at low temperatures. They are easy to be scaled up to an industrial level, but they suffer from the disadvantage that the particles are sometimes less crystalline and more polydispersed because of the slow nucleation rate at low reaction temperatures. On the other hand, organometallic-based syntheses have been widely adopted recently to synthesize particles with high crystallinity and monodispersity. These methods involve the high-temperature thermal decomposition of zero-valent organometallic precursors or the reduction of metal salts in high-boiling solvents in the presence of stabilizing ligands. The high reaction temperature (150−300 °C) facilitates the removal of crystalline defects and results in high-quality magnetic nanoparticles. However, the toxicity of the solvents, ligands and precursors used in these types of syntheses might limit their applications to a certain extent [21].

2.1. Microemulsion approaches

A microemulsion is a thermodynamically stable dispersion of two relatively immiscible liquids stabilized by surfactant molecules [22]. Depending on relative concentrations, surfactant molecules self-assemble into a variety of structures in the solvent mixture, such as micelles, bilayers and vesicles. Most commonly used structures in nanoparticle synthesis are micelles, either as reverse (water-in-oil) or normal (oil-in-water) form. In both cases, the dispersed phase consists of monodispersed droplets in the size range of 2–100 nm. This dispersed phase provides a confined environment for synthesizing nanoscale particles [23]. Fig. 1 shows several strategies to synthesize metal nanoparticles [24]. Early pioneering work by Boutonnet et al. showed microemulsions of water/cetyltrimethylammonium bromide (CTAB)/octonal and water/pentaethyleneglycol dodecyl ether/hexane can be used to dissolve metal ions, and subsequently be reduced by hydrogen or hydrazine, resulting in the formation of monodispersed

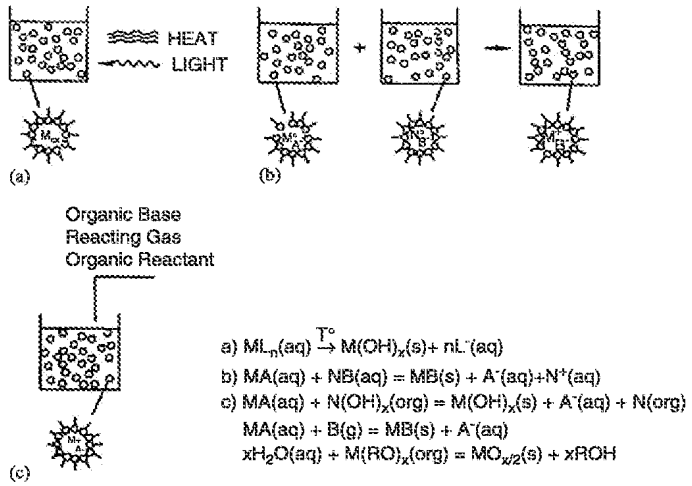

Fig. 1. Several strategies to synthesize nanoparticles using reverse micelle synthesis: (a) hydrolysis induced by light or heat; (b) displacement reaction involving mixing two different micellar solutions; (c) reducing metal salt using an organic base or other reactants. Reproduced with permission from Ref. [24].

Pt, Pd, Rh and Ir nanoparticles [25]. Borohydride reduction of cobalt chloride in water/didodecyldimethyl ammonium bromide (DDAB)/toluene results in the formation of Co nanoparticles [26–28]. Temperature affects the aggregation states of micelles, and thus induces finite aggregates of nanoparticles when the reaction is carried out at elevated temperatures [29]. The final product is very sensitive to the concentration of water in the system. With a high concentration of water, metal boride Co_2B or Ni_2B particles form instead of pure metallic particles [30]. Another micelle system that has been widely used in nanoparticle synthesis consists of water/sodium bis(2-ethylhexyl)sulfosuccinate (AOT)/alkane. The water droplets formed by AOT in alkane have a small degree of polydispersity, and the micelle size can be accurately controlled by the composition ratio w(= [water]/[AOT]) [31]. Pileni et al. have used AOT micelles to synthesize a variety of transition metal particles, including, Cu, Co [32,33]. O'Connor et al. also used AOT micelles to synthesize a series of ferrite particles, MFe_2O_4, (M = Co, Mn, Fe) [34].

Normal micelles formed in an aqueous solution can also be used to control the particle growth. In this case, the spherical micelles act as nucleation centers for the growing particles. Mixing micellar solutions of cobalt dodecyl sulfate ($Co(DS)_2$) and iron dodecyl sulfate ($Fe(DS)_2$) led to the formation of $CoFe_2O_4$ nanoparticles [35,36]. Further coating with silica made the particles bio-compatible and could potentially be functionalized with biomolecules for drug delivery and cell separation [37].

2.2. Organometallic synthesis

Thermal decomposition and reaction of organometallic precursors at high temperatures have been quite successful

in generating highly monodispersed magnetic nanoparticles. This is because nucleation at a high temperature occurs almost instantaneously, thus the particle growth stage is well separated from the initial nucleation event.

Decomposition of metal carbonyls have been used to generate ferrofluids for quite sometime [38,39]. But it is only recently that the degree of control in these syntheses has been substantially improved. Using trioctylphosphine oxide (TOPO) as a surface ligand, Dinega et al. showed that the decomposition of $[Co_2(CO)_8]$ yielded nanoparticles with ε-phase, a distorted face-centered-cubic (FCC) structure that is absent in the bulk cobalt [40]. Similarly, the thermal decomposition of iron pentacarbonyl, $Fe(CO)_5$, produced iron nanoparticles using TOPO as a solvent. Subsequent oxidation by a chemical reagent led to the formation of monodispersed maghemite nanoparticles [41]. The extraordinary control of particle size distribution within 1 nm was demonstrated recently using iron–oleate complex as precursor (Fig. 2) [42,43]. A typical strategy adapted in these syntheses is to utilize a pair of ligands that have different binding affinities. A tightly binding ligand will favor slow growth, while a weakly coordinating ligand will promote rapid growth. By adjusting the ratio of these two types of ligands, the nanoparticle size can be regulated. Alivisatos and co-workers described the formation of cobalt nanodisks and particles using TOPO and oleic acid (OA) as ligands [44,45].

Alternatively, reducing agents are added to metal salt solutions at a high temperature to generate magnetic nanoparticles. Using this approach, Murray and co-workers have synthesized cobalt nanoparticles with different crystal structures through the high-temperature reduction of cobalt salts [46]. The injection of superhydride ($LiEt_3BH$) into a hot solution of cobalt chloride in dioctyl ether (set at 200 °C) in the presence of OA and trialkylphosphine resulted in the formation of ε-phase Co nanoparticles. By changing the steric bulkiness of the stabilizing surface ligands, they were able to control the Co nanoparticle size from 2 to 11 nm. The use of short-chain alkylphosphines allowed faster growth and resulted in bigger particles, while the bulkier ligands favor the formation of smaller nanoparticles by retarding the particle growth. Subsequent heating of the ε-Co nanoparticles at 300 °C under vacuum converted them to the hexagonal-close-packed (HCP)-Co, which has a higher magnetocrystalline anisotropy than that of the ε-phase.

The same group also prepared HCP-Co nanoparticles directly by using the polyol process, in which a high boiling alcohol was used both as reducing agent and solvent. In a typical synthesis, 1,2-dodecanediol was added into a hydrated cobalt acetate solution in diphenyl ether, which contained OA and trioctylphosphine at 250 °C to produce cobalt nanoparticles [47]. By using nickel acetate as a metal precursor, nickel nanoparticles with particle sizes in the range of 8–13 nm could also be obtained. A similar high-temperature reaction of iron(III) acetylacetonate in phenyl ether in the presence of alcohol and surfactant was used to make monodisperse magnetite nanoparticles [48].

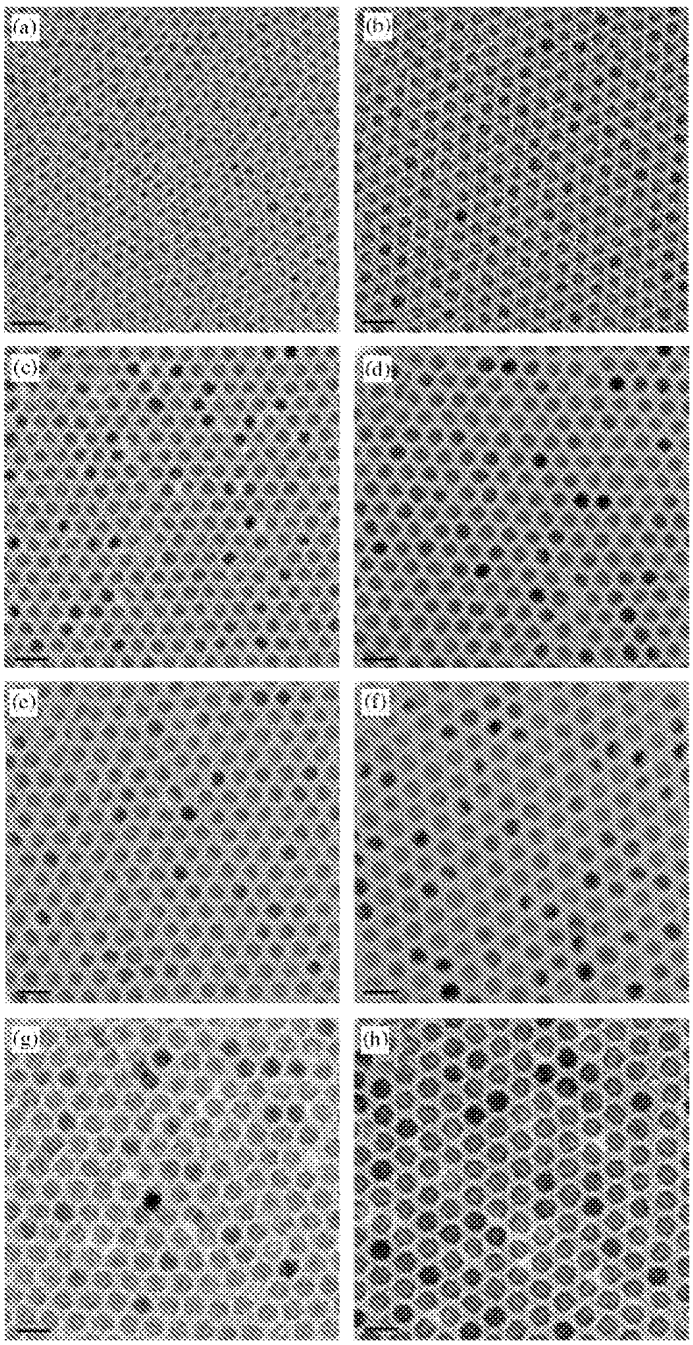

Fig. 2. Transmission electron microscopy (TEM) images of (a) 6-, (b) 7-, (c) 8-, (d) 9-, (e) 10-, (f) 11-, (g) 12-, and (h) 13-nm-sized air-oxidized iron oxide nanoparticles showing the 1 nm level increments in diameter. Reproduced with permission from Ref. [42].

Alloy particles were made using two different organometallic precursors in the same reaction. Highly monodispersed Fe_xPt_{1-x} nanoparticles were synthesized by simultaneous decomposition of $Fe(CO)_5$ and reduction of platinum acetylacetonate ($Pt(acac)_2$) in the presence of polyol reducing agents [49]. The Fe and Pt compositions in

these particles are readily tuned by controlling the molar ratio of $Fe(CO)_5$ and $Pt(acac)_2$ [50]. The as-prepared Fe_xPt_{1-x} particles have the FCC structure, which is magnetically soft. After annealing at temperatures higher than 650 °C, the particles are converted to the magnetic hard $L1_0$ phase. Co-reduction of an iron and $Pt(acac)_2$ precursor also yield 2 and 4 nm FePt particles [51–53]. Reduction of $Pt(acac)_2$ and thermal decomposition of cobalt carbonyl in the presence of 1-adamantanecarboxylic acid were employed in different coordinating mixtures to produce monodispersed, highly crystalline $CoPt_3$ nanoparticles. The mean particle size was varied from 1.5 to 7.2 nm by controlling the reaction conditions [54]. Recent X-ray absorption experiments (XAS) on Co–Pt core–shell nanoparticles have shown that the existing Co particles can induce a redox transmetalation reaction with $Pt(acac)_2$, and form a Pt shell on its surface. Subsequent interatomic diffusion of Pt atoms into the interior of the particles at elevated temperatures resulted in the formation of CoPt alloy particles [55]. Thus, the reducing agent (1,2-hexadecanediol) in the original synthesis is not absolutely necessary. CoNi alloy nanoparticles were also produced using a mixture of cobalt acetate and nickel acetate through a similar synthetic approach. In a similar synthesis, FePd nanoparticles were synthesized [56].

Thermal decomposition can also be induced by sonication [57]. Sonolysis of a solution of $Fe(CO)_5$ in anisol in the presence of poly(dimethylphenylene oxide) (PPO) formed small iron particles [58]. Laser-induced pyrolysis of $Fe(CO)_5$ led to pure γ-Fe particles deposited into organic solvents with sizes ranging from 30 to 85 nm [59]. Oxides and ferrites can also be produced by controlled oxidation of metal or metal alloy particles obtained by thermal decomposition. The diameter of the particles is tunable from 3 to 20 nm by varying reaction conditions or by seed-mediated growth [41,60,61].

2.3. *Effect of ligands and particle shape control*

Surface ligands or surfactants provide stabilizing organic shells that mediate the nanoparticle solubility, prevent aggregations and limit surface oxidation. Small magnetic clusters can be stablized by small ligands, such as CO or pyridine. Large ferromagnetic particles, on the other hand, have to be stabilized by sterically bulky ligands in order to prevent them from agglomeration due to the strong magnetic interactions. Co particles with size of 27 nm were synthesized in toluene using staresorcinarene tetraphosphonite as ligand [62]. These large particles form ring structures spontaneously upon solvent evaporation in order to achieve magnetic flux closure. Ligand exchange reactions have been used to change the hydrophobicity of the particles synthesized in the organic phase. For instance, a mixed monolayer of poly(ethylene glycol)-terminated thiol and dopamine ligands were used to replace oleic acid capped FePt particles. A highly charged surface ligands results in great stability of the particle in water and even in a cell culture medium [63].

Ligand molecules also play an important role in controlling the particle growth, and in many cases, can determine the shape and structure of final products. Surfactant molecules in reverse micelles are believed to be loosely bound to the nanoparticle surface. However, experiments on Fe showed surfactants with a different charge head group can affect the internal structure. In particular, nonionic surfactant tetraethyleneglycol dodecyl ether ($C_{12}E_4$) induced FCC γ-Fe, while cationic DDAB induced α-Fe nanoparticles [64]. Combined with carboxylic acids, long-chain amines were shown to be capable of inducing nanorod and nanowire formation. The simultaneous decomposition of bis(cyclooctadiene)nickel(0) [$Ni(COD)_2$] and tetraphenyldibismuthine [Bi_2Ph_4] in tetrahydrofuran (THF) at the refluxing temperature led to nickel–bismuth alloy nanoparticles with an average size of 8–10 nm. When the decomposition was carried out at a higher temperature (200 °C) in the presence of trioctylamine and OA, NiBi nanowires were observed in addition to the nanoparticles [65]. In a different experiment, cobalt, nickel nanorods and nanowires, with different aspect ratios, were obtained through the decomposition of organometallic precursors in the presence of a mixture of long-chain amines and OA [66]. A slow injection of Fe-TOP complex into octyl ether and oleylamine at 300 °C induced Fe_2P nanorod formation (Fig. 3) [67]. Another procedure that yield Fe nanorods was through reflux heating of small 2 nm spherical Fe particles synthesized by $Fe(CO)_5$ decomposition in pyridine solvent with DDAB as surfactant [68].

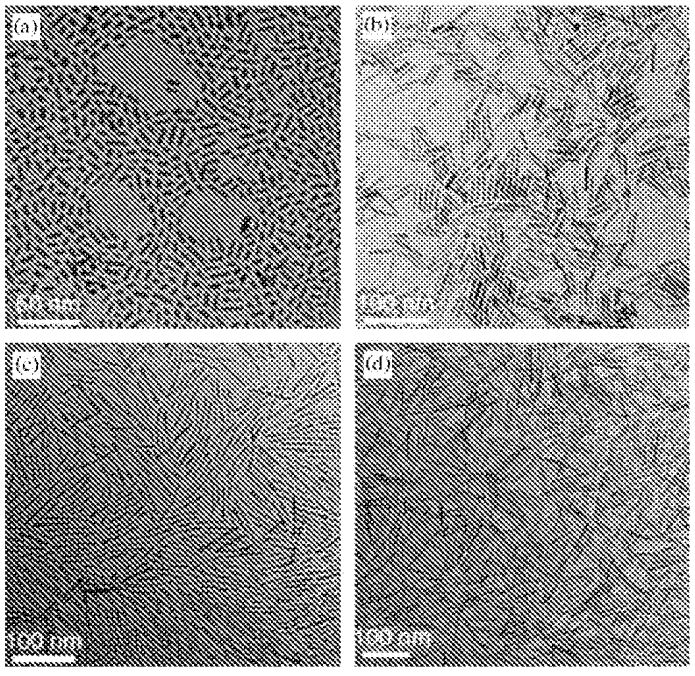

Fig. 3. TEM images of iron phosphide nanorods: (a) 3 × 12 nm; (b) 5 × 43 nm; (c) 5 × 88 nm; (d) 6 × 107 nm. Reproduced with permission from Ref. [67].

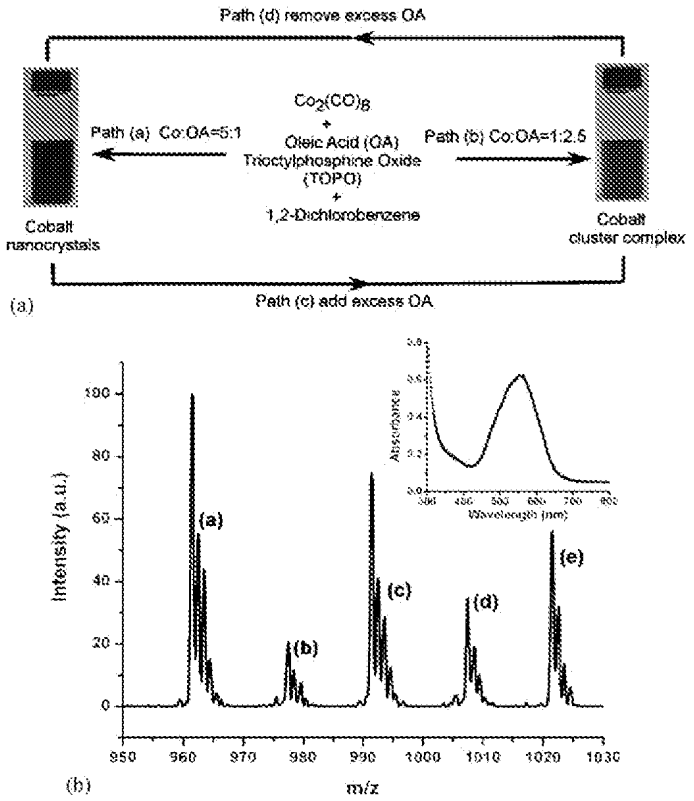

Fig. 4. (a) Schematic diagram illustrating the experimental procedures to synthesize cobalt NCs and cluster complexes using different concentrations of OA ligand. (b) Electro-spray mass spectrum of the cobalt cluster complex in 1,2- dichlorobenzene. The mass of the peaks correspond to Co_2OA_3, Co_3OA_3 cluster complex. Inset shows the UV–Vis absorbance of the cluster solution. Reproduced with permission from Ref. [69].

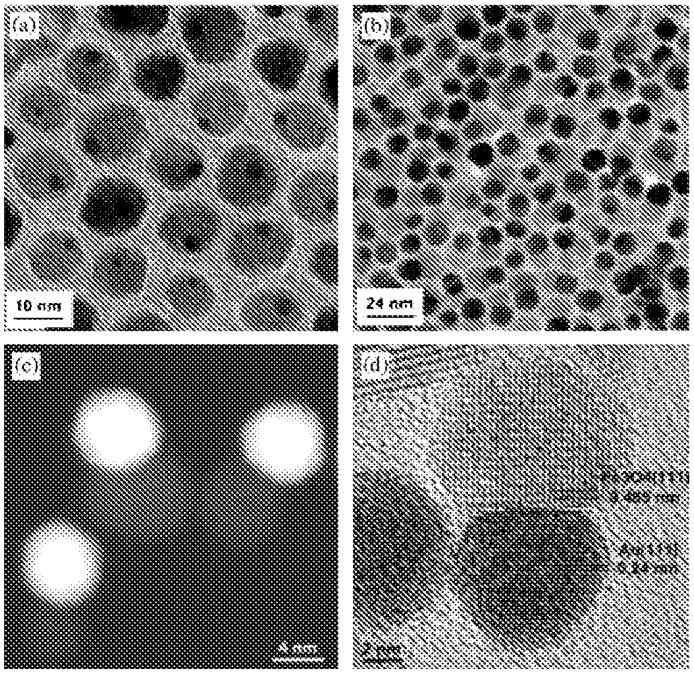

Fig. 5. TEM images of the dumbbell-like Au–Fe_3O_4 nanoparticles: (a) 3-14 nm Au–Fe_3O_4 particles; (b) TEM image of the 8–14 nm Au–Fe_3O_4 particles; (c) high-angle annular dark field scanning transmission electron microscopy (HAADF-STEM image) 8–9 nm Au–Fe_3O_4 particles; and (d) high-resolution TEM image of one 8–12 nm Au–Fe_3O_4 particle. Reproduced with permission from Ref. [74].

The concentration of the ligand also affects the reaction pathways. Different concentrations of OA ligands during the cobalt carbonyl decomposition resulted in the formation of either large ferromagnetic nanocrystals (NCs) or small cluster complex that showed antiferromagentic coupling (Fig. 4) [69]. More dramatically, by adding or removing free oleic acid ligands from the final reaction product, NC colloid could be turned into a cluster complex solution and vice versa. The fact that Co_2 and Co_3 clusters are possible intermediate building blocks for constructing large NCs could explain why the ε-phase instead of the FCC or HCP phase was observed in these syntheses.

2.4. Composite particles

Composite particles made of several different materials introduce multicomponents in a single particle, and thus possibly, new physical properties. By combining a high-temperature decomposition route with seed-mediated growth, core–shell particles were formed with ferrimagnetic spinel ferrite $CoFe_2O_4$ coated with a shell of the antiferromagnet MnO. The composite showed a shifted hysteresis loop as a result of the exchange bias between the core and shell structures [70]. Bimagnetic core/shell $Fe_{58}Pt_{42}/Fe_3O_4$ nanoparticles were synthesized from a high-temperature solution phase. Magnetic properties of the as-synthesized core/shell particles depended on the shell thickness due to the exchange coupling between core and shell [71].

Combining nanoscale magnets with a semiconductor or a noble metal could lead to nanocomposite materials with better magneto-optical responses. Co/CdSe core/shell nanocomposites were prepared by controlled CdSe deposition onto pre-formed Co NCs [72]. Dumbbell shape heterostructure NC composites consisting of iron oxide particles and either semiconductor [73] or noble metal particles [74] as a second component have recently been synthesized (Fig. 5). The formation of these structures was attributed to the large lattice mismatch of the junction [73] or the charge polarization on the interface [74]. These heterostructures were shown to have retained the optical and magnetic properties of the individual components, permitting potential applications in bioassays that rely on both the magnetic and optical responses.

3. Self-assembly

Colloidal NCs self-assemble into two-dimensional (2D) and three dimensional (3D) superlattices spontaneously, upon evaporation of solvent [46,75]. The self-assembly is driven by isotropic van der Waals interactions between particles and the steric repulsions due to ligand interdigitation. For particles that are superparamagnetic at room

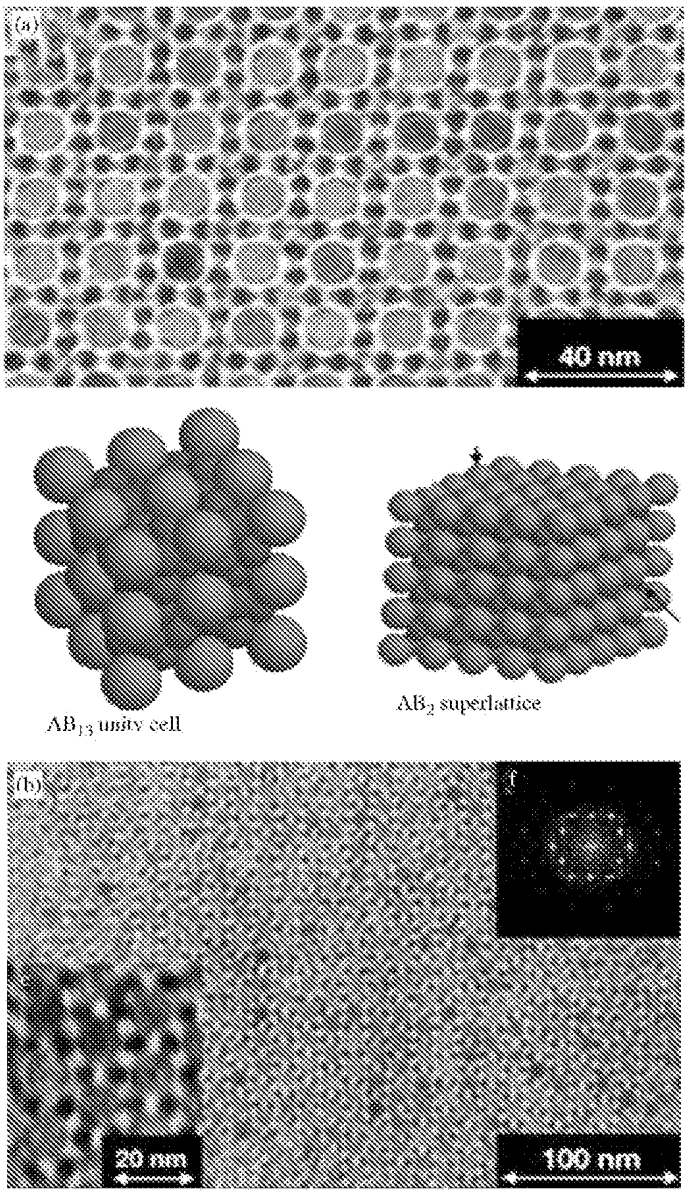

Fig. 6. (a) Projection of a {1 0 0} plane of AB_{13} superlattice made of 11 nm Fe_2O_3 and 6 nm PbSe NCs. (b) Projection of the (0 0 1) plane of AB_2 superlattice built up of alternating layers of 11 nm Fe_2O_3 and 6 nm PbSe NCs. Reproduced with permission from Ref. [80].

temperature, magnetic interactions between particles are also isotropic, thus superparamagnetic particles behave more or less similar to nonmagnetic nanoparticles.

One of the early studies on iron oxide supercystals using TEM was carried out by Bentzon et al. [76]. They demonstrated HCP superstructures up to 5–10 layers were formed from the intensity of the X-ray generated from exposing the sample with an electron beam. Using a combination of bright field imaging and projected potential simulations, Majetich et al. were able to identify different crystal packing structures in multilayer superlattices [77]. If the colloidal evaporation occurs under an applied magnetic field, stripes and needle shape superlattices are usually formed, reflecting the competition between alignment of magnetic moment with fields and long-range magnetostatic interactions between particles [46].

For evaporation-induced self-assembly, a narrow size distribution of the building blocks is not the only parameter required to achieve long-range order. Other conditions, such as composition of the dispersing solvent, temperature and evaporation kinetics, also play very important roles. Rapid drying (<10 s) of a Ni nanoparticle (9 nm) solution onto an amorphous carbon TEM grid from pentane, resulted in the formation of a close-packed glassy assembly. While deposition of the same sample from 80% hexane and 20% octane, which slowed the evaporation time to $\sim$5 min, resulted to an ordered Ni nanoparticle superlattice growth [78]. Furthermore, the wetting properties of the substrate was shown to influence the nanoparticle superlattice morphology. The superlattice growth was more 2D if the nanoparticle dispersion wetted the substrate, initially forming a monolayer and adding subsequent layers as the coverage was increased. However, the resulting superlattice adapted a more 3D character when the nanoparticle dispersion did not wet the substrate.

Binary systems made of different sizes of particles typically form phase separated regions during self-assembly. However, with selected size ratios, binary AB, AB_2, AB_5 or AB_{13} colloidal crystals can form spontaneously. Ordered monolayers created by mixing two sizes of $CoPt_3$ NCs displayed the binary AB_2 or AB composition, and a trilayer formed AB_5 structure [79]. Mixing two sizes of 11 nm Fe_2O_3 and 6 nm PbSe NCs produced binary superlattices of AB_{13} and AB_2 structures (Fig. 6) [80]. In these multicomponent NC assemblies, the properties of each component may be engineered individually. By tuning the coupling between different functionalities, it might be possible to engineer complex structures with desired properties.

Layer-by-layer (LBL) deposition is another self-assembly technique that can create complex superstructures. It involves using opposite charged polyelectrolytes to assemble multilayers of nanoparticles of different types. Magnetic luminescent nanocomposites were prepared via the LBL assembly approach. The Fe_3O_4 magnetic nanoparticles of 8.5 nm were used as a template for the deposition of the CdTe quantum dots (QDs)/polyelectrolyte (PE) multilayers [81].

Magnetic NCs have also been synthesized in situ in other self-assembled matrices [82]. Diblock copolymer polystyrene-block-poly(2-vinylpyridine) (PS-b-PVP) forms spherical inverse micelles in toluene. The inverse micelles loaded with cobalt chloride were self-assembled on a substrate to form 2D arrays. Subsequent oxygen plasma etching removed the polymer coating and resulted in Co_3O_4 particle arrays on the surface. Hydrogen plasma etching converted these oxide particles back to pure Co particles, as was demonstrated by in situ photoelectron spectroscopy. One advantage of this self-assembly technique is that the interparticle spacing can be tuned by the chain length of the

polymer. Similar experiments were carried out by mixing thiolated gold colloid with a solution of polystyrene-b-poly (4-vinylpyridine), which formed hexagonally ordered micelles upon evaporation. Gold NCs preferentially distributed themselves in the polystyrene coronas. When the $FeCl_3$ precursor embedded in the PVP domains was oxidized, Fe_2O_3 particles formed in the PVP cores, thus creating a binary NC superlattice [83]. An inorganic matrix can also be used to assemble magnetic nanoparticle particles. Cobalt nanoparticles were incorporated into hexagonal honeycomb mesoporous silica [84]. The nanoscale confinement in 1D pores led to ferromagnetic coupling between particles, which was evident from the increased coercivity.

4. Physical properties

The electronic band structure of materials in the nanometer region is strongly affected by quantum confinement and high surface/bulk ratio. The magnetic moment of a nanoparticle, which results from both the spin moments and orbital moments, is closely related to its electronic structure. Size-dependent magnetic properties for individual nanoparticles as well as the coupling between the nanoparticles have been the main focus of physical property investigation of magnetic nanoparticles.

4.1. Single particle properties

For ferromagnetic transition metals, the magnetic moments originate from the itinerant d-band electrons. For small particles with high surface-to-volume ratio, reduced coordination leads to enhanced magnetic moments for the surface atoms. This was demonstrated by Stern–Gerlach experiments in the gas phase [3,4]. In the case of chemically synthesized NCs, there have been only a few reports of enhanced magnetic moments in transition metal nanoparticles [85–87]. Even with these reported cases, the ambiguity remains whether the observed enhancement could be attributed to absorbed ions or the effect of surface ligands [87,88]. In other cases, quenched magnetic moments [46] were observed due to the formation of oxides or a possible electron transfer from surface ligands to metal surface atoms [89]. Another way to control the magnetic properties of individual particles is to modify the surface by different materials. Exchange coupling between magnetically soft Fe_3O_4 shell and magnetically hard FePt core was shown to create a large coercivity as well as a high saturation magnetization for the composite particles [71].

Collective excitation of magnetic moments creates spin waves. In bulk materials, this leads to a decrease of the magnetization with temperature according to Bloch's law $M(T) = M_0[1 - BT^b], b = \frac{3}{2}$. In magnetic nanoparticles, the spin wave spectrum can become quantized due to the finite particle size. Direct measurements of spin wave quantization effects have so far been limited to template grown nanowires [7] and submicron lithographically patterned dots [6,90] and stripes [91] where the sizes of the magnetic features are much larger than the characteristic length scale in magnetic materials. For particles on the order of a few nanometers or a few tens of nanometers, direct evidences of spin wave quantization are still lacking. However, the temperature dependence of the saturation magnetization on chemically synthesized core–shell [Mg]Fe, $[MgF_2]$Fe particles showed a strong deviation from Bloch's law when the particle diameter is below 15 nm (Fig. 7), which indicates that quantization effects could be pronounced when the particle sizes are below 10 nm [92].

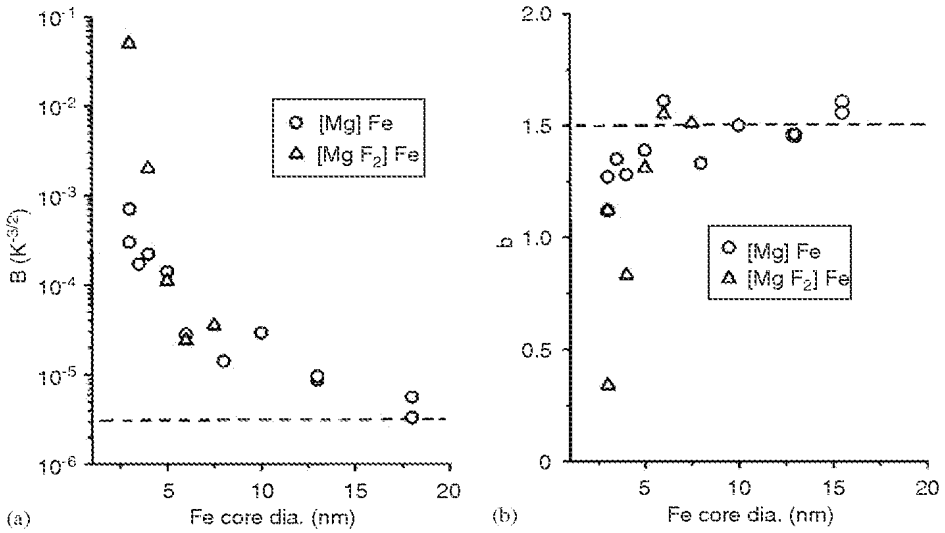

Fig. 7. Bloch constant (a) and Bloch exponent (b) as a function of iron crystal size for both Mg and MgF_2 coated Fe nanoparticles. Reproduced with permission from Ref. [92].

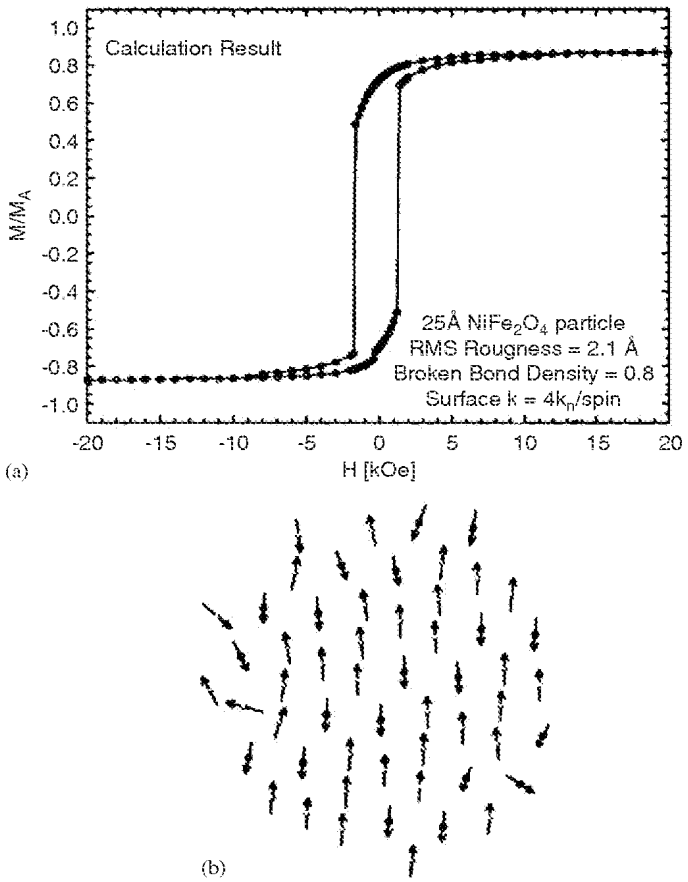

Fig. 8. (a) Calculated hysteresis loops for a 2.5 nm $NiFe_2O_4$ particle and (b) corresponding spin configurations. Reproduced with permission from Ref. [95].

The dynamic response of magnetic moments under a changing field is an important parameter for nanoparticles used in magnetic storage applications [19]. At high temperatures, magnetic moment switching occurs through a thermally activated process, thus the magnetization relaxes exponentially when the magnetic field is switched off, $M(t) = M_0 e^{-\Gamma t}$, with Γ being the decay rate given by $\Gamma = \Gamma_0 e^{-U/k_B T}$. For a system with a broad distribution of barrier heights U, the magnetization relaxes in a logarithmic form, $M(t) = M_0(1 - n(\overline{E})k_B T \ln(t/t_0))$. The viscosity term $S = n(\overline{E})k_B T$ measures how fast the system is responding to the changing field. At very low temperatures when the thermal activation is suppressed, macroscopic quantum tunneling (MQT) becomes an important mechanism for moment switching [93]. This is manifested in a temperature-independent viscosity S. Such behavior was indeed discovered in the $CoFe_2O_4$ system [94]. However, it has been argued by Kodama et al. that a complex barrier distribution with $n(\overline{E}) = 1/E$ can also lead to temperature-independent viscosity as well [19]. Such complex energy barrier distributions can be introduced by particle size dispersion as well as the surface anisotropy originated from spin disorder on the particle surface [19]. Fig. 8 shows the calculated hysteresis loop and magnetic moment distribution of a 2.5 nm $NiFe_2O_4$ particle [95]. The spin disorder on the particle surface is a direct result of exchange bonds breaking for the surface atoms.

4.2. Collective properties

In closed packed nanoparticle arrays, exchange coupling and dipolar interactions both lead to collective magnetic behavior that extend beyond a single particle. Experimentally, it is still difficult to vary the relative strength of these interactions systematically. What further complicates the issue is the random distribution of magnetic easy axes in the arrays even though the physical structures might look highly ordered. Monte Carlo simulations by Kechrakos and Trohido showed that, for 3D random assembly of interacting nanoparticles coupled via exchange and dipolar forces, the coercivity decreases with concentration for all values of the exchange strength. The concentration dependence of the remanence is determined by the competition between the two types of interactions and the crossover occurs when the strengths are comparable. The blocking temperature increases with concentration, except when particle coalescence occurs and the system is above the percolation limit [96,97]. These predictions explained the variety of different behavior observed in experiments [98–102].

A more complicated scenario involves assemblies of particles with vastly different intrinsic properties. Binary assembly of FePt and Fe_3O_4 particles were formed by mixing the particles with appropriate size ratio [103]. Subsequent annealing converted the assembly into FePt–Fe_3Pt nanocomposites. Similar to core–shell composites [74], an optimum exchange coupling between neighboring grains enhances the overall energy product of the system. The optimum coupling can be obtained by independently tuning the size and composition of the individual building blocks. These exchanged coupled spring magnets systems have shown great promise in future generations of high-performance magnets.

The effect of long-range dipole–dipole interactions on the relaxation dynamics has been a subject of considerable interests during the last decade. Under a weak interparticle interaction, the effect can be accounted for by a change of the energy barriers of the isolated particles [104,105]. When the interactions are sufficiently strong, there is a possibility of collective spin-glass-like behavior in random interacting systems. Magnetic relaxation measurements in Fe–C nanoparticles showed a critical slowing down at a finite temperature [106]. Nonlinear susceptibility showed a divergent behavior using static scaling [107]. These experiments exhibit strong evidence that spin-glass behavior exists in a strongly coupled nanoparticle system. There is, however, a major difference between atomic spin glass with the magnetic particles with dipolar interactions [107]. For atomic spin glass, the flip time of the individual magnetic moment is of the order of 10^{-13} s and is independent of temperature, while in magnetic nanoparticle systems, the

moment flip time can vary from nanoseconds to geological time scales according to $\tau = \tau_0 e^{-KV/k_B T}$, where τ_0, 10^{-12}~10^{-9} s, KV is the anisotropy energy, and $k_B T$ is the thermal energy. The distribution of anisotropy energies inevitably implies a distribution of flip times of the individual magnetic moments. Memory effects observed in ($Ni_{81}Fe_{19}$) [108] and Fe_2O_3 [109] nanoparticles have been attributed to the distribution of magnetic moment switching times rather than the cooperative nature of the magnetic moments.

5. Summary and future directions

Colloidal chemistry has generated and will continue to create magnetic nanostructures with high monodispersity, well-controlled sizes, unique shapes and complex structures. Compared with the top-down lithographic technique, it has the advantage to achieve small particle size and unmatched structural complexity. There are, however, many challenges ahead in this field. For magnetic storage applications, the stability of nanoparticle media under thermal annealing needed to induce the $L1_0$ phase transformation remains a problem, although impurity doping of the as-prepared particles has made some progress [110,111]. Self-assembly of magnetic building blocks on the macroscopic length scale with nanometer precision is still a technically challenging task. For a 2D assembly, one possible solution might be inducing symmetry breaking by assembling the magnetic NCs at the liquid–air interface, which has already been demonstrated in noble metal nanoparticles [112]. Having magnetic easy axes aligned in a large assembly is crucial for storage media. Anisotropic particles, such as cubic-shaped particles are likely to have their easy axes aligned in one of the primary crystal axes, and therefore could be useful in that respect. To achieve well-controlled particle shape, the mechanism of surface ligands in controlling the particle growth needs to be further investigated. Another area that has shown great promise is composite particles made from several different materials with multi-functionalities. Magnetic relaxation of individual particles and assemblies needs to be further studied with high spatial and temporal resolutions.

This work is supported by the US Department of Energy (DOE), BES-Materials Sciences, under Contract #W-31-109-ENG-38.

References

[1] A. Aharoni, Introduction to the Theory of Ferromagnetism, Clarendon Press, Oxford, 2001.
[2] R. Skomski, J. Phys. 15 (2003) R841.
[3] J.P. Bucher, D.C. Douglass, L.A. Bloomfield, Phys. Rev. Lett. 66 (1991) 3052.
[4] I.M.L. Billas, A. Châtelain, W.A. De Heer, Science 265 (1994) 1682.
[5] E.E. Fullerton, J.S. Jiang, C.H. Sowers, J.E. Pearson, S.D. Bader, Appl. Phys. Lett. 72 (1998) 380.
[6] S. Jung, B. Watkins, L. DeLong, J.B. Ketterson, V. Chandrasekhar, Phys. Rev. B 66 (2002) 132401.
[7] U. Ebels, J.-L. Duvail, P.E. Wigen, L. Piraux, L.D. Buda, K. Ounadjela, Phys. Rev. B 64 (2001) 144421.
[8] A.E. Berkowitz, J.R. Mitchell, M.J. Carey, A.P. Young, S. Zhang, F.E. Spada, F.T. Parker, A. Hutten, G. Thomas, Phys. Rev. Lett. 68 (1992) 3745.
[9] J.Q. Xiao, J.S. Jiang, C.L. Chien, Phys. Rev. Lett. 68 (1992) 3749.
[10] D.A. Thompson, J.S. Best, IBM J. Res. Dev. 44 (2000) 311.
[11] D. Weller, A. Moser, IEEE Trans. Mag. 35 (1999) 4423.
[12] R.D. Shull, IEEE Trans. Mag. 29 (1993) 2614.
[13] L.X. Tiefenauer, G. Kuehne, R.Y. Andres, Bioconjugate Chem. 4 (1993) 347.
[14] M. Beller, H. Fischer, K. Kuhlein, C.-P. Reisinger, W.A. Herrmann, J. Organometal. Chem. 520 (1996) 257.
[15] C.R. Martin, P. Kohli, Nat. Rev. Drug Dis. 2 (2003) 29.
[16] D.L. Leslie-Pelecky, R.D. Rieke, Chem. Mater. 8 (1996) 1770.
[17] K.A. Easom, K.J. Klabunde, C.M. Sorensen, G.C. Hadjipanayis, Polyhedron 13 (1994) 1197.
[18] T. Hyeon, Chem. Commun. 8 (2003) 927.
[19] R.H. Kodama, J. Mag. Mag. Mater. 200 (1999) 359.
[20] J.L. Dormann, I. Fiorani, Magnetic Properties of Fine Particles, North-Holland, Amsterdam, 1992.
[21] Z.A. Peng, X. Peng, J. Am. Chem. Soc. 123 (2001) 168.
[22] J.N. Israelachvili, Intermolecular and Surface Forces, Academic Press Ltd., San Diego, 2003.
[23] M.P. Pileni, J. Phys. Chem. B 105 (2001) 3358.
[24] K. Osseo-Asare, F.J. Arriagada, in: G.L. Messing, S. Hirano, H. Hausner (Eds.), Ceramic Powder Science, vol. III, American Ceramic Society, 1990, p. 3.
[25] M. Boutonnet, J. Kizling, P. Stenius, G. Maire, Colloids Surf. 5 (1982) 209.
[26] G.N. Glavee, K.J. Klabunde, C.M. Sorensen, G.C. Hadjipanayis, Inorg. Chem. 32 (1993) 474.
[27] X.M. Lin, C.M. Sorensen, K.J. Klabunde, G.C. Hajipanayis, J. Mater. Res. 14 (1999) 1542.
[28] J.P. Wilcoxon, J.E. Martin, P. Provencio, Langmuir 16 (2000) 9912.
[29] X.M. Lin, C.M. Sorensen, K.J. Klabunde, G.C. Hajipanayis, Langmuir 14 (1998) 7140.
[30] J.B. Nagy, I. Bodart-Ravet, E.G. Derouane, Farad. Discuss. Chem. Soc. 87 (1989) 189.
[31] J. Eastoe, B.H. Robinson, D.C. Steytler, D. Thorn-Lesson, Adv. Colloid. Inter. Sci. 36 (1991) 1.
[32] M.P. Pileni, Adv. Funct. Mater. 11 (2001) 323.
[33] C. Petit, A. Taleb, M.P. Pileni, J. Phys. Chem. B 103 (1999) 1805.
[34] C.T. Seip, E.E. Carpenter, C.J. O'Connor, V.T. John, S. Li, IEEE Trans. Mag. 34 (1998) 1111.
[35] A.J. Rondinone, A.C.S. Samia, Z.J. Zhang, J. Phys. Chem. B 104 (2000) 7919.
[36] A.J. Rondinone, A.C.S. Samia, Z.J. Zhang, J. Phys. Chem. B 103 (1999) 6876.
[37] C.R. Vestal, Z.J. Zhang, Nano. Lett. 3 (2003) 1739.
[38] C.H. Griffiths, M.P. O'Horo, T.W. Smith, J. Appl. Phys. 50 (1979) 7108.
[39] T.W. Smith, D. Wychick, J. Phys. Chem. 84 (1980) 1621.
[40] D.P. Dinega, M.G. Bawendi, Angew. Chem., Int. Ed. Engl. 38 (1999) 1788.
[41] T. Hyeon, S.S. Lee, J. Park, Y. Chung, H.B. Na, J. Am. Chem. Soc. 123 (2001) 12798.
[42] J. Park, E. Lee, N.-M. Hwang, M. Kang, S.C. Kim, Y. Hwang, J.-G. Park, H.-J. Noh, J.-Y. Kim, J.-H. Park, T. Hyeon, Angew. Chem. Int. Ed. 44 (2005) 2872.
[43] J. Park, K. An, Y. Hwang, J.-G. Park, H.-J. Noh, J.-Y. Kim, J.-H. Park, N.-M. Hwang, T. Hyeon, Nat. Mater. 3 (2004) 891.
[44] V.F. Puntes, K.M. Krishan, A.P. Alivisatos, Appl. Phys. Lett. 78 (2001) 2187.

[45] V.F. Puntes, K.M. Krishan, A.P. Alivisatos, Science 291 (2001) 2115.
[46] C.B. Murray, S. Sun, H. Doyle, T. Betley, MRS Bull. (2001) 985.
[47] C.B. Murray, S. Sun, W. Gaschler, H. Doyle, T.A. Betley, C.R. Kagan, IBM J. Res. Dev. 45 (2001) 47.
[48] S. Sun, H. Zeng, J. Am. Chem. Soc. 124 (2002) 8204.
[49] S. Sun, C.B. Murray, D. Weller, L. Folks, A. Moser, Science 287 (2000) 1989.
[50] S. Sun, E.E. Fullerton, D. Weller, C.B. Murray, IEEE Trans. Magn. 37 (2001) 1239.
[51] K.E. Elkins, T.S. Vedantam, J.P. Liu, H. Zeng, S. Sun, Y. Ding, Z.L. Wang, Nano Lett. 3 (2003) 1647.
[52] C. Liu, X. Wu, T. Klemmer, N. Shukla, X. Yang, D. Weller, A.G. Roy, M. Tanase, D. Laughlin, J. Phys. Chem. B 108 (2004) 6121.
[53] S. Sun, S. Anders, T. Thomson, J.E.E. Baglin, M.F. Toney, H.F. Hamann, C.B. Murray, B.D. Terris, J. Phys. Chem. B 107 (2003) 5419.
[54] E.V. Shevchenko, D.V. Talapin, A.L. Rogach, A. Kornowski, M. Haase, H. Weller, J. Am. Chem. Soc. 124 (2002) 11480.
[55] J.-I. Park, M.G. Kim, Y.-W. Jun, J.S. Lee, W.-R. Lee, J. Cheon, J. Am. Chem. Soc. 126 (2004) 9072.
[56] M. Chen, D.E. Niles, J. Appl. Phys. 91 (2002) 8477.
[57] K.S. Suslick, S.B. Choe, A. Cichowlas, M. Grinstaff, Nature 353 (1991) 414.
[58] D. de Caro, T. Ould-Ely, A. Mari, B. Chaudret, E. Snoeck, M. Respaud, J.-M. Broto, A. Fert, Chem. Mater. 8 (1996) 1987.
[59] X.Q. Zhao, F. Zheng, Y. Liang, Z.Q. Hu, Y.B. Xu, Mater. Lett. 21 (1994) 285.
[60] T. Hyeon, Y. Chung, J. Park, S.S. Lee, Y.-W. Kim, B.H. Park, J. Phys. Chem. B 106 (2002) 6831.
[61] S. Sun, H. Zeng, D.B. Robinson, S. Raoux, P.M. Rice, S.X. Wang, G. Li, J. Am. Chem. Soc. 126 (2004) 273.
[62] S.L. Tripp, S.V. Pusztay, A.E. Ribbe, A. Wei, J. Am. Chem. Soc. 124 (2002) 7914.
[63] R. Hong, N.O. Fischer, T. Emrick, V.M. Rotello, Chem. Mater. 17 (2005) 4617.
[64] J.P. Wilcoxon, P.P. Provencio, J. Phys. Chem. B 103 (1999) 9809.
[65] T. Ould-Ely, J.H. Thurston, A. Kumar, M. Respaud, W.H. Guo, C. Weidenthaler, K.H. Whitmire, Chem. Mater. 17 (2005) 4750.
[66] N. Cordente, M. Respaud, F. Senocq, M.-J. Casanove, C. Amiens, B. Chaudret, Nano Lett. 1 (2001) 565.
[67] J. Park, B. Koo, Y. Hwang, C. Bae, K. An, J.-G. Park, H.M. Park, T. Hyeon, Angew. Chem. Int. Ed. 43 (2004) 2282.
[68] S.-J. Park, S. Kim, S. Lee, Z.G. Khim, K. Char, T. Hyeon, J. Am. Chem. Soc. 122 (2000) 8581.
[69] A.C.S. Samia, K. Hyzee, J.A. Schlueter, C.-J. Qin, J.S. Jiang, S.D. Bader, X.M. Lin, J. Am. Chem. Soc. 127 (2005) 4126.
[70] O. Masala, R. Seshadri, J. Am. Chem. Soc. 127 (2005) 9354.
[71] H. Zeng, J. Li, Z.L. Wang, J.P. Liu, S. Sun, Nano. Lett. 4 (2004) 187.
[72] H. Kim, M. Achermann, L.P. Balet, J.A. Hollingsworth, V.I. Klimov, J. Am. Chem. Soc. 127 (2005) 544.
[73] K.-W. Kwon, M. Shim, J. Am. Chem. Soc. 127 (2005) 10269.
[74] H. Yu, M. Chen, P.M. Rice, S.X. Wang, R.L. White, S. Sun, Nano. Lett. 5 (2005) 379.
[75] C.P. Collier, T. Vossmeyer, J.R. Heath, Annu. Rev. Phys. Chem. 49 (1998) 371.
[76] M.D. Bentzon, J. van Wonterghem, S. Mørup, A. Thölén, Philos. Mag. B 60 (1989) 169.
[77] S. Yamamuro, D.F. Farrell, S.A. Majetich, Phys. Rev. B 65 (2002) 224431.
[78] C.B. Murray, C.R. Kagan, M.G. Bawendi, Annu. Rev. Mater. Sci. 30 (2000) 545.
[79] E.V. Shevchenko, D.V. Talapin, A.L. Rogach, A. Kornowski, M. Haase, H. Weller, J. Am. Chem. Soc. 124 (2002) 11480.
[80] F.X. Redl, K.-S. Cho, C.B. Murray, S. O'Brien, Nature 423 (2003) 968.
[81] X. Hong, J. Li, M. Wang, J. Xu, W. Guo, J. Li, Y. Bai, T. Li, Chem. Mater. 16 (2004) 4022.
[82] H.-G. Boyen, G. Kästle, K. Zürn, T. Herzog, F. Weigl, P. Ziemann, O. Mayer, C. Jerome, M. Möller, J.P. Spatz, M.G. Garnier, P. Oelhafen, Adv. Funct. Mater. 13 (2003) 359.
[83] B.-H. Sohn, J.-H. Choi, S.I. Yoo, S.-H. Yun, W.C. Zin, J.C. Jung, M. Kanehara, T. Hirata, T. Teranishi, J. Am. Chem. Soc. 125 (2003) 6368.
[84] A.F. Gross, M.R. Diehl, K.C. Beverly, E.K. Richman, S.H. Tolbert, J. Phys. Chem. B 107 (2003) 5475.
[85] J.P. Chen, C.M. Sorensen, K.J. Klabunde, G.C. Hadjipanayis, Phys. Rev. B 51 (1995) 11527.
[86] J. Osuna, D. de Caro, C. Amiens, B. Chaudret, E. Snoeck, M. Respaud, J.-M. Broto, A. Fert, J. Phys. Chem. 100 (1996) 14571.
[87] J.P. Wilcoxon, E.L. Venturini, P. Provencio, Phys. Rev. B 69 (2004) 172402.
[88] X.M. Lin, unpublished data.
[89] D.A. van Leeuwen, J.M. van Ruitenbeek, L.J. de Jongh, A. Ceriotti, G. Pacchioni, O.D. Häberlen, N. Rösch, Phys. Rev. Lett. 73 (1994) 1432.
[90] G. Gubbiotti, G. Carlotti, R. Zivieri, F. Nizzoli, T. Okuno, T. Shinjo, J. Appl. Phys. 93 (2003) 7607.
[91] J. Jorzick, S.O. Demokritov, B. Hillebrands, M. Bailleul, C. Fermon, K.Y. Guslienko, A.N. Slavin, D.V. Berkov, N.L. Gorn, Phys. Rev. Lett. 88 (2002) 047204.
[92] D. Zhang, K.J. Klabunde, C.M. Sorensen, G.C. Hadjipanayis, Phys. Rev. B 58 (1998) 14167.
[93] J. Tejada, R.F. Ziolo, X.X. Zhang, Chem. Mater. 8 (1996) 1784.
[94] X.X. Zhang, J.M. Hernàndez, J. Tejada, R. Solé, X. Ruiz, Phys. Rev. B 53 (1996) 3336.
[95] R.H. Kodama, A.E. Berkowitz, Phys. Rev. B 59 (1999) 6321.
[96] D. Kechrakos, K.N. Trohidou, J. Mag. Mag. Mater. 262 (2003) 107.
[97] D. Kechrakos, K.N. Trohidou, Phys. Rev. B 58 (1998) 12169.
[98] J.L. Dormann, L. Bessais, D. Fiorani, J. Phys. C 21 (1988) 2015.
[99] S. Gangopadhyay, G.C. Hadjipanayis, C.M. Sorensen, K.J. Klabunde, IEEE Trans. Magn. 29 (1993) 2619.
[100] S. Mørup, E. Tronc, Phys. Rev. Lett. 72 (1994) 3278.
[101] R.V. Chamberlin, J. Hemberger, A. Loidl, K.D. Humfeld, D. Farrell, S. Yamamuro, Y. Ijiri, S.A. Majetich, Phys. Rev. B 66 (2003) 172403.
[102] P. Poddar, T. Telem-Shafir, T. Fried, G. Markovich, Phys. Rev. B 66 (2002) 060403.
[103] H. Zeng, J. Li, J.P. Liu, Z.L. Wang, S. Sun, Nature 420 (2002) 395.
[104] J.L. Dormann, D. Fiorani, E. Tronc, Adv. Chem. Phys. 98 (1997) 283.
[105] D. Fiorani, J. Tholence, J.L. Dormann, J. Phys. C 19 (1986) 5495.
[106] C. Djurberg, P. Svedlindh, P. Nordblad, M.F. Hansen, F. Bødker, S. Mørup, Phys. Rev. Lett. 79 (1997) 5154.
[107] T. Jonsson, P. Svedlindh, M.F. Hansen, Phys. Rev. Lett. 81 (1998) 3976.
[108] Y. Sun, M.B. Salamon, K. Garnier, R.S. Averback, Phys. Rev. Lett. 91 (2003) 167206.
[109] G.M. Tsoi, U. Senaratne, R.J. Tackett, E.C. Buc, R. Naik, P.P. Vaishnava, V.M. Naik, L.E. Wenger, J. Appl. Phys. 97 (2005) 10J507.
[110] O. Kitakami, Y. Shimada, K. Oikawa, H. Daimon, K. Fukamichi, Appl. Phys. Lett. 78 (2001) 1104.
[111] S. Kang, J.W. Harrell, D.E. Nikles, Nano. Lett. 2 (2002) 1033.
[112] S. Narayanan, J. Wang, X.M. Lin, Phys. Rev. Lett. 93 (2004) 135503.